Characterization of large area, thick, and segmented silicon detectors for neutron β-decay experiments

A. Salas-Bacci[a,b,*], P. L. McGaughey[b], S. Baeßler[a,d], L. Broussard[e], M. F. Makela[b], J. Mirabal[b], R. W. Pattie[c], D. Počanić[a], S. K. L. Sjue[b], S. I. Penttila[d], W. S. Wilburn[b], A. R. Young[c], B. A. Zeck[c], Z. Wang[b]

[a] *University of Virginia, Charlottesville, VA, USA, 22904*
[b] *Los Alamos National Laboratory, Los Alamos, NM, USA, 87545*
[c] *North Carolina State University, Raleigh, North Carolina, USA, 27695*
[d] *Oak Ridge National Laboratory, Oak Ridge, TN 37831*
[e] *Duke University, Durham, NC 27708*

Abstract

The "Nab" and "UCNB" collaborations have proposed to measure the correlation parameters in neutron β-decay at Oak Ridge and Los Alamos National Laboratory, using a novel detector design. Two large area, thick, hexagonal-segmented silicon detectors containing 127 pixels per detector will be used to detect the proton and electron from neutron decay. Both silicon detectors are connected by magnetic field lines of a few Tesla field strength, and set on an electrostatic potential, such that protons can be accelerated up to 30 keV in order to be detected. Characteristics of the detector response to low energy conversion electrons and protons from 15 keV to 35 keV, including the evaluation of the dead layer thickness and other contributions to the pulse height defect for proton detection are presented for Si detectors of 0.5 mm and 1 mm of thickness.

Keywords: neutron beta decay, silicon detector, pulse height defect, nuclear defect, dead layer

---

1. Introduction

Neutron beta decay, one of the most fundamental processes in nuclear physics, offers a unique opportunity to test the basics of the weak interaction, and to test certain limits of the standard model (SM) of elementary particles and fields. Thanks to extraordinary theoretical precision, SM calculations of the neutron beta decay and its observables have reached precision levels of a few parts in 10^4, surpassing the available experimental precision by up to an order of magnitude (0.13% for τ_n, 0.2% for λ). As an additional challenge to the experimental comunity, there are significant inconsistencies in the world data set on several

*Corresponding author
Email address: americo.salas.bacci.1@ohio.edu (A. Salas-Bacci)

key properties of the neutron: $\tau_{\rm n}$, its lifetime, and $\lambda = g_A/g_V$, the nucleon axial vector form factor (for recent summaries see Refs. [1, 2]). The importance of precise knowledge of the observables in neutron decay (lifetime, as well as the various decay correlations), cannot be overemphasized, as they play an important role in setting limits on non-$(V-A)$ interaction terms (and therefore new, non-SM physics), and have significant implications in astrophysics.

For all the above reasons, several new experimental initiatives were recently proposed with the aim to measure precisely several neutron decay parameters: a, the electron-neutrino correlation, b, the Fierz interference term, A, the beta asymmetry, as well as B and C, the neutrino and proton asymmetries, respectively. These quantities are defined by the expressions for the differential neutron beta decay rate:

$$\frac{\mathrm{d}w}{\mathrm{d}E_e \mathrm{d}\Omega_e \mathrm{d}\Omega_\nu} \propto p_e E_e (E_0 - E_e)^2 \times \left[1 + a \frac{\vec{p}_e \cdot \vec{p}_\nu}{E_e E_\nu} + b \frac{m_e}{E_e} + \langle \vec{\sigma}_n \rangle \cdot \left(A \frac{\vec{p}_e}{E_e} + B \frac{\vec{p}_\nu}{E_\nu} + \ldots \right) \right], \tag{1}$$

and, for the proton asymmetry,

$$C = \kappa(A + B) \qquad \text{where} \qquad \kappa \simeq 0.275\,. \tag{2}$$

The planned new experiments are: Nab, to measure a and b at the Spallation Neutron Source (SNS), Oak Ridge National Laboratory [3, 4], UCNB [5], to measure B at Los Alamos National Laboratory, and abBA [6], and PANDA [7], to measure A, C, and B, also at the SNS. Traditionally, A has been measured precisely; the new experiments offer independent means to measure λ. While Nab, abBA and PANDA detect decays of cold neutrons, UCNB uses ultracold neutrons. Common to all of these experiments is that, unlike some prior ones, they detect both electrons and protons in coincidence from neutron decay, and measure their energies. This technique opens the possibility to specify each event kinematically, thus allowing measurements of correlations involving neutrinos, and greatly improves the suppression of backgrounds. Both improvements are critical to realizing a new generation of precision measurements of the neutron decay parameters.

The collaborations have jointly set out to develop a specialized large-area Si detector capable of detecting both 30 keV protons and electrons up to 1 MeV kinetic energies [5, 6]. Figure 1 shows the set-up of the detectors in the Nab spectrometer. The 12 cm diameter detectors are segmented into 127 hexagonal pixels, and are 2 mm thick in order to stop the highest energy neutron beta decay electrons produced in the spectrometer decay volume. A key detector property is its thin, < 100 nm thick, dead layer. However, low energy proton detection is complicated even with such an advanced device as this new detector. This paper discusses in detail the various systematic effects arising in detection of 30 keV proton with

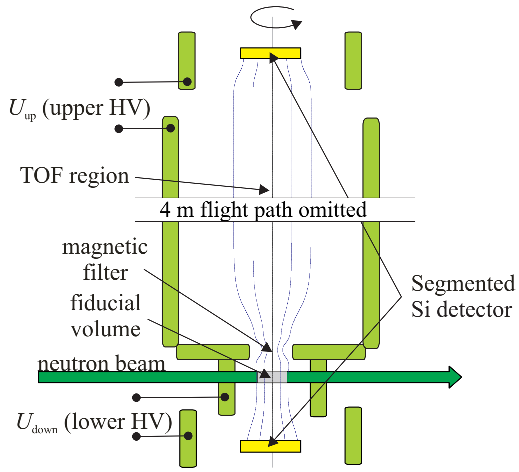

Figure 1: Schematic design of Nab spectrometer. Protons are accelerated in a field of U_{up}=-30 kV in order to be detected by the top large area 127-hexagonal segmented Si detector. The strength of the magnetic field varies between 4 T and 0.1 T in the filter and TOF region. Electrons and protons are constrained to spiral along the magnetic field lines. The bottom Si detector is immersed in -1 kV field. The highest energy electrons are stopped and detected by either 2 mm thick detectors.

the large area, 0.5 mm and 1 mm, thick segmented Si detectors, focusing on the measured pulse height defect that has to be properly accounted for in any precision measurement.

2. Segmented large-area silicon detector

2.1. Detector

The silicon detectors are produced from single 12 cm diameter wafers of single-crystal silicon 0.5 mm, 1 mm, and 2 mm thick [8]. The detectors are ion-implanted to form diode structures and produced using standard photo-lithography techniques. Charged particles enter through the front (p-implant) side, that consists of a shallow implant layer with a very fine (0.4% of active area) aluminum grid to provide electrical conductivity. The square grid lines are 10 μm wide and spaced 4 mm apart. The detector has an entrance window of $<$ 100 nm silicon-equivalent thickness, as shown in Figure 2. Charges are collected from the back (ohmic) side of the detector, which is segmented into 127 hexagonal pixels measuring 8.9 mm side-to-side, with an area of 70 mm^2 each and separated by 100 μm. The total active area of the detector, including partial pixels at the edge, is 108 cm^2.

Detection of protons with small area ($\leq$ 600 mm^2) or thin Si detectors (SBD, SDD) in neutron decay can be found elsewhere [9, 10, 11, 12, 13, 14, 15].

2.2. Front-end amplifier

Given the aim to detect low energy protons, the front-end amplifier was designed to have the following characteristics: 1) high gain, 2) low noise, 3) fast risetime, 4) large dynamic range and, 5) moderate cost. To meet these goals, a charge sensitive amplifier consisting of a cooled FET stage, followed by a pre-amplifier and post-amplifier was implemented using

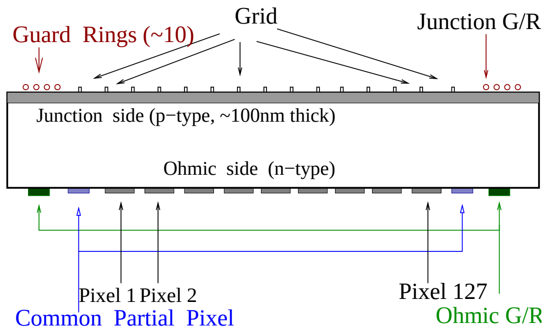

Figure 2: A cross section view of the silicon detector. The Si wafer is 12 cm in diameter. The planned experiments will be carried out with 2 mm thick detectors. The 16.6 cm diameter ceramic disc that is attached on the ohmic side of the Si wafer is not shown in the figure.

commercially available components, as shown in Figure 3. A BF862 low-noise FET was chosen with input capacitance to roughly match that of a silicon pixel. The BF862 has $0.8\,\mathrm{nV}/\sqrt{\mathrm{Hz}}$ input noise at 100 kHz and a gate capacitance of 10 pF. A common source FET circuit was chosen, with the drain signal amplified by an AD8011 pre-amplifier. A 1 pF feedback capacitor (C1) from the amplifier output to the FET gate completed the charge integrator. A $1\,\mathrm{G}\Omega$ resistor (R2) served to discharge the integrator. Some output overshoot was removed by providing a small amount of negative feedback to the inverting input (C4). The output from the AD8011 also drove an AD8099 post-amplifier, with a fixed voltage gain of 20. An interstage coupling capacitor (C3) between them acted as high pass filter. Likewise, high frequency noise was removed by a low pass filter (L1,C5). Component values were optimized using SPICE simulations using device parameters from the manufacturers. Bench testing confirmed the expected noise ($\sim 1.3\,\mathrm{nV}/\sqrt{\mathrm{Hz}}$ at 22 pF input capacitance), gain and bandwidth of the electronics. The FET was mounted directly on the silicon detector and cooled to $-6°$C in vacuum. The remainder of the electronics was operated at room temperature outside the vacuum chamber. Coaxial cables were used to connect the input and feedback sections of the pre-amplifier and FET. The post-amplifier was connected to an Ortec 672 shaping amplifier, with a gain of 5 and shaping time of 1 usec. The shaped signal was digitized by an Amptek MCA-8000A multichannel analyzer. An overall system gain of $\sim$100 mV/fC was obtained with a measured noise of $\sigma \sim 1.3$ keV silicon energy equivalent. This performance allowed for efficient detection of 15 keV protons with low background rate.

2.3. Detection of 30 keV protons

In both Nab and UCNB experiments, protons from neutron beta-decay are accelerated first through a 30 kV potential drop for detection. Our capabilities of low energy proton detection with 0.5 mm and 1 mm thick detectors were studied at the proton accelerator laboratory at the Triangle Universities Nuclear Laboratory (TUNL) [16]. Prior to the proton detection, we have investigated low deposited energy detection with two different detector thicknesses, 0.5 mm and 1 mm, using alpha sources of ^{241}Am, and ^{148}Gd, and conversion electron sources of ^{113}Sn, ^{139}Ce, and principally ^{109}Cd. The detection of 62.5 keV electrons, $\sim$22 keV X-rays from ^{109}Cd reflected a continuous improvement in the signal-to-noise ratio

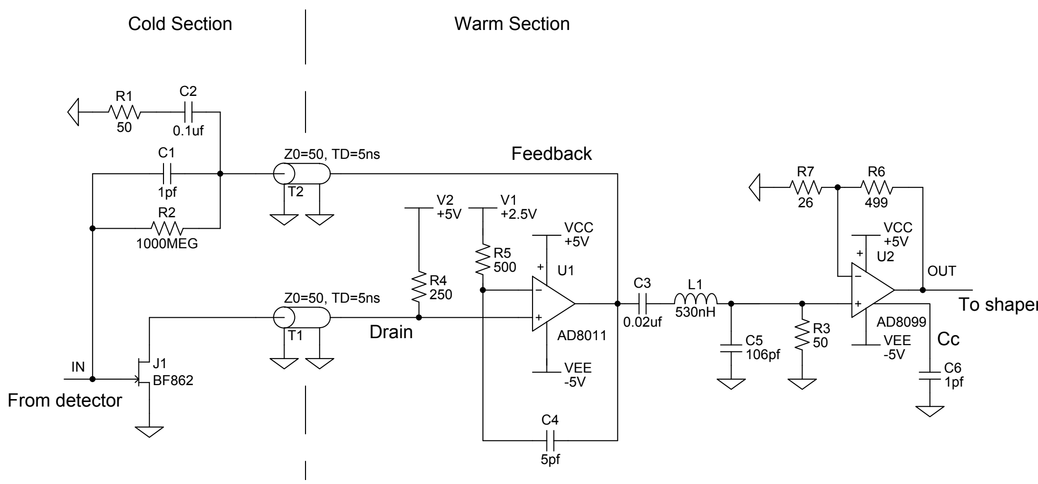

Figure 3: Pre-amplifier schematic described in Section 2.2.

which prepared our detector and instrumentation for 30 keV proton detection that is one of the main requirements of detector performance. A proton of 30 keV produces less than $\sim 6 \times 10^3$ electron-hole pairs in the active volume of the detector. The first step in improving the detection of low deposited energy was to decrease the bulk leakage current to $\lesssim$ 1nA/pixel which was achieved by cooling the detector to $-6°$C. Figure 4 shows the measured bulk leakage current as a function of the bias voltage. The temperature of the detector was controlled by coupling the detector support to Cu tubing that was cooled by circulating antifreeze liquid as is shown in Figure 5. To verify the temperature of the detector an identical dummy detector was cooled with four temperature sensors mounted on the surface of the detector. The detector was operated in darkness inside the vacuum chamber with unnecessary instrumentation such as pressure gauges and temperature sensors turned off.

Successful measurement of the ^{109}Cd spectrum was only possible after reducing instrumental noise using a variety of techniques: the detector bias voltage was provided by a battery, ground loops were avoided by using a single grounding point, the FET was directly mounted on the pixel pin to avoid capacitive couplings, the stainless steel vacuum chamber protected the detector against electromagnetic noise, a metal mesh inside the vacuum pipe of the chamber minimized the mechanical noise, and electronic filters, and very low noise pre and post amplifiers were connected using short coaxial cables at appropiate points in the circuitry.

Direct detection of 30 keV protons with our silicon detectors requires a stable low intensity proton accelerator, capable of providing $\sim 300\, s^{-1}$ of protons with energies lower than 40 keV, and a beam energy resolution of ≈ 0.6 keV (FWHM). This accelerator was built at TUNL by members of the UCNA collaboration [17]. The main features of the accelerator are described by Hoedl and Young [16]. For the proton detection with our detector, the small vacuum chamber shown in Figure 5 was connected to the grounded and electrically insulated high energy end of TUNL accelerator. The thickness of the vacuum chamber pro-

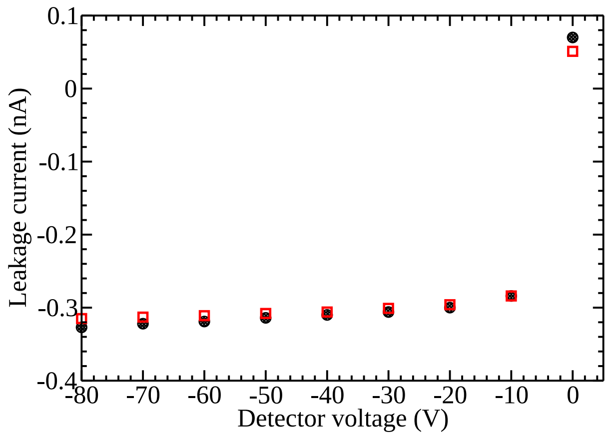

Figure 4: Leakage current as a function of the bias voltage for pixel number 63 (circle) and number 64 (square) of the large area 1.0 mm thick silicon detector at $-6°C$. Pixel number 64 is the central pixel of the detector while the pixel number 63 is an adjacent pixel. For proton detection the detector was operated at $-75V$.

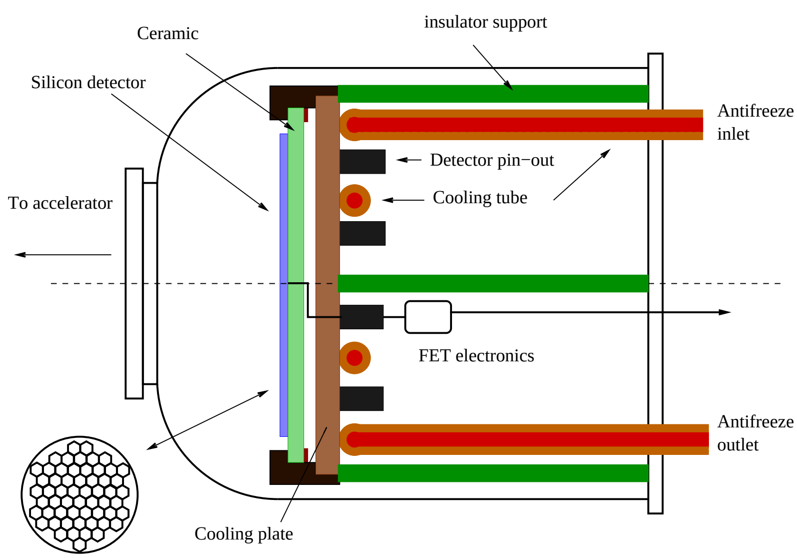

Figure 5: A cross section schematic of the detector assembly inside of the vacuum chamber. The Si detector is attached on a ceramic disc of 16.6 cm diameter and 1 mm thickness which provides both structural support for cooling the detector, and electrically insulates the wafer. Part of the hexagonal detector segmentation is shown at the bottom left of the schematic.

vided a sufficient skin depth to shield the detector and FET from electromagnetic radiative couplings. The large area, thick, segmented silicon detector was supported inside the chamber by electrical insulators made from PEEK material and the assembly was firmly coupled to the 16.5” vacuum flange in the way that the central pixel was in the middle of the beam, however we could also detect ions with the adjacent pixels, especially with the ones located above and below the central pixel or beam center. The chamber was evacuated to 10^{-6} Torr by a dry pump station before cooling down the detector to avoid contaminating the detector surface.

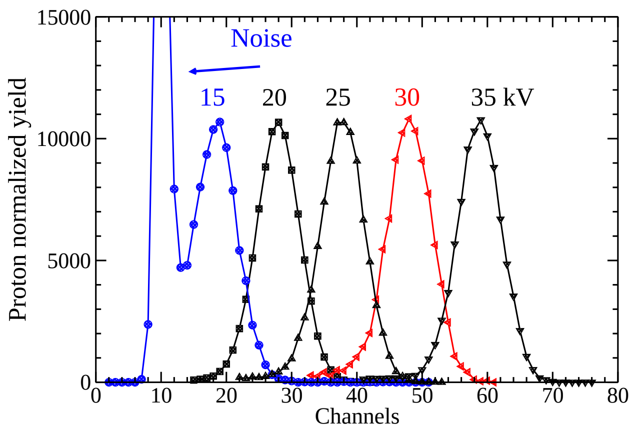

Figure 6: Detection of low energy protons with 1 mm thick silicon detector at $-6°$C. The proton acceleration voltage (in kV) is shown next to each peak. Protons are detected after crossing the detector dead layer. The average detected energy resolution is 3.2 keV (FWHM). A threshold was set to the MCA to cut the noise.

Figure 6 shows the results of low energy proton detection. The initial goal was only to detect 30 keV protons, however, given that we had already detected $\sim$ 22 keV X-Rays from ^{109}Cd, it was possible to detect protons down to 15 keV. From the energy calibration with ^{109}Cd described in section 3 we obtain that E=(0.411×ch+1.56)keV which gives a noise level of 6.1 keV corresponding to ch=11 in Figure 6. A similar result for the noise level is obtained with deuterons, shown in Figure 7. The lowest proton energy detected with the 0.5 mm thick detector corresponds to 22 keV, limited by detector capacitance, shown in Figure 8. The total evaluated detector capacitance of 0.5 mm, 1 mm, and 2 mm thick detectors is about 2 nF, 1 nF, and 0.5 nF, respectively, which gives 15.7, 7.9, and 3.9 pF/pixel for 127-hexagonal segmented detector. The proton detection for Nab and UCNB experiments will be carried out with the 2 mm thick silicon detectors, which will even further reduce noise.

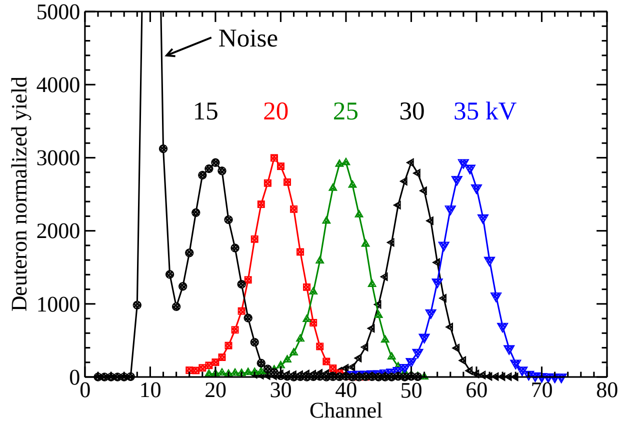

Figure 7: Low energy deuteron detection with 1 mm thick silicon detector at $-6°$C. The deuteron acceleration voltage (in kV) is shown next to each peak. Deuterons are detected after crossing the dead layer.

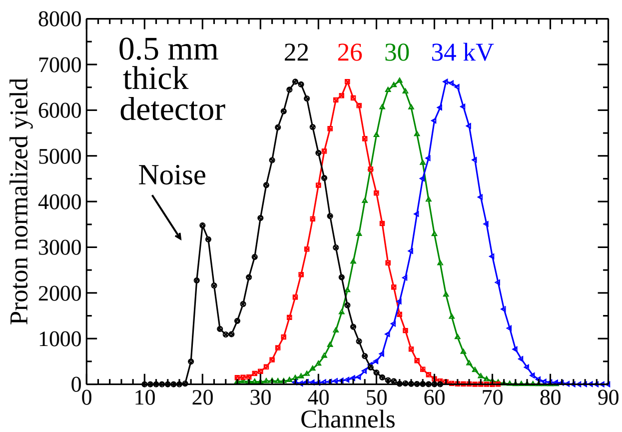

Figure 8: Low energy proton detection with 0.5 mm thick silicon detector at $-6°$C. The proton acceleration voltage (in kV) is shown next to each peak. Protons are detected after crossing the dead layer. The measured average energy resolution is 5.5 keV (FWHM). The corresponding noise level for ch=21 is 10 keV.

3. Simulation of a ^{109}Cd spectrum in silicon detector

As an alternative method to characterize the Si detector for detection of low deposited energy, we have measured the spectra of ^{109}Cd for energy calibration and to determine the pulse height defect associated with proton and deuteron detection. In order to use conversion electrons from ^{109}Cd source we first need to determine the spectrum incident on the Si detector.

The source of ^{109}Cd with 8.11 nCi of beta activity has a holder diameter of 25 mm and an active source diameter of 3 mm with a mylar cover and support of 3.5 μm thickness. The source mounted on a copper holder was placed ∼10 cm away from the central pixel of the detector that was operated under the same conditions as in the proton detection. The measured ^{109}Cd spectrum was affected by energy loss in the mylar cover; to correct the spectrum it was necessary to simulate the detector response using a PENELOPE [18] based Monte Carlo simulation.

In the simulation, a 1 cm radius mylar foil of thickness which was varied from ∼3.5 μm-12 μm was positioned 10 cm away from the 1 mm thick silicon disk, backed by an Al disk. The source foil was mounted on an Al ring, having a 1 mm×1 mm square cross section, which was placed in front of a 2 mm thick copper plate. All objects had cylindrical symmetry and were coaxial with the z-axis. In the model the first 100 nm of the silicon detector was considered "dead" and therefore the energy loss in this volume was tallied separately.

Events were generated according to the probabilities of relative emission intensities for ^{109}Cd [19] within a 1.5 mm radius in the center of the source foil with an isotropic momentum distribution. One million events were generated for each geometry that was investigated. Events were tracked until the primary and all secondary particles either exited the system or were absorbed when their energies fell below 100 eV.

A measured background-subtracted ^{109}Cd spectrum was used in the data analysis to verify the simulation results. The measured background was scaled to match the low energy peak in the data and fit to an exponential which was then subtracted from the original spectrum. A separate calibration was also carried out with a pulse generator with variable amplitude output to provide a voltage vs. MCA units of calibration.

The quality of the measured and simulated energy spectra after voltage calibration by the pulse generator was quantified by a minimum χ^2 test. Figure 9 shows the result of this comparison, while numerical values indicate that a mylar foil thickness of 6.0 μm matches best the data.

Systematic effects from source tilt and detector misalignment were also modeled. If the source mount was tilted, the path length, l, in the foil would increase by $\Delta l = l/\cos\theta - l$ which increases the energy loss of the conversion electrons. To simulate this effect to first order the mylar foil thickness was varied between 1.5 μm to 6.5 μm. There are two notable effects of the mylar foil thickness on the recorded energy in the detector shown in Figure 10, the electron peaks at 18 keV, 63 keV, and 84 keV shift to lower voltages as the thickness increases and the X-ray peak at ≈22 keV is unaffected by foils. Another cross-check of the mylar foil thickness, the expectation that above a thickness of 2.5 μm, the 18 keV Auger line falls below our noise threshold, was also confirmed in our ^{109}Cd measurement. A series of

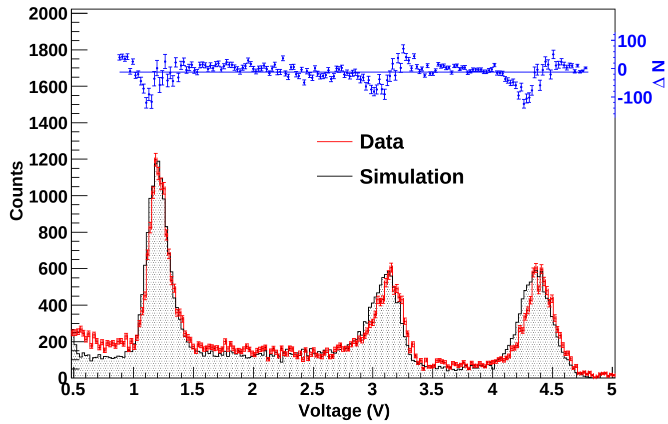

Figure 9: A 6.0 μm thick mylar foil gives the best fit to the data. Shown in red is the background subtracted data, while the black filled area is the simulated energy spectrum. The residuals, ΔN, are shown at the upper part of the figure.

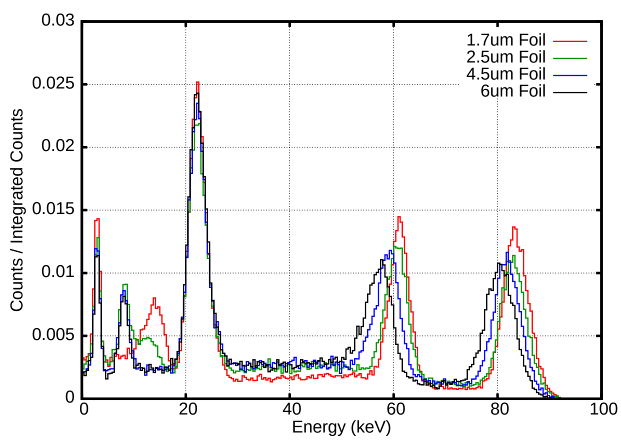

Figure 10: The simulated ^{109}Cd spectra with four mylar foil thicknesses of 1.7 μm -6.0 μm. Increasing the mylar foil thickness causes a change in the intensity for $\approx$22 keV X-rays and the thicker films shift the conversion electron peaks to lower energies and increase the multiple scattering tails of those distributions.

larger simulations were run with 14 million events for a few of the mylar foil thicknesses to investigate the effect of source-detector misalignment. Radial position cuts, r=1 cm, at y=0, 2, 3, 4, 5, and 6 cm along the y-axis were used to mimic the source being offset of the "active" region of the detector. The maximum effect of the "offset" is just 2 keV (2%) shift in the conversion peaks, the X-ray peak unchanged.

4. Pulse height defect of low energy protons

It is well known that charged particles of different species with the same kinetic energy, E_0, recorded with the same detector produce different response, expressed in terms of its pulse height (PH). As $PH \propto E_0$, it is common to define the pulse height defect (PHD) as $\Delta E_{PHD} = E_0 - E'$, where E' is the detected energy. The PHD is specially important for heavy ions, and it is also relevant for low-Z particles at low kinetic energies. The PHD is considered to include three terms: $\Delta E_{PHD} = \Delta E_{\rm w} + \Delta E_{\rm n} + \Delta E_{\rm r}$, where $\Delta E_{\rm w}$ is known as the "window defect", if it is given in units of energy, or as the "dead layer" if expressed in units of length. The dead layer is the detector region where the charge from ionization is not collected. The second term, $\Delta E_{\rm n}$, is the so called nuclear defect (strictly speaking atomic scattering defect), discussed in section 5 with a value of $\Delta E_{\rm n}$= 0.8 keV for 30 keV protons. The third term, $\Delta E_{\rm r}$, is the recombination defect which is originated by the incomplete collection of charges by the electric field applied to the detector due to a recombination of electron-holes in the created plasma.

Based on three arguments, the recombination defect of our Si detector is insignificant compared with the other two defects. The first argument is operational, the detector has been operated at a reverse bias voltage higher than the recommended value. The operating point was determined by varying the bias and observing the centroid for the main line of ^{241}Am, and at the same time monitoring that the leakage current did not exceeded $\sim$1 nA/pixel. For a reverse bias higher than 72V the alpha centroid of 5485 keV reached a saturation value with a clearly defined plateau. This indicated that the detector internal electric field was sufficient to collect all the electron-hole pairs produced by the incident particle with minimal recombination. On the other hand, for a detector diode temperature of -6°C, a reverse bias of 75 V produces a leakage current of 0.32 nA/pixel, that is a resistivity of 1.7×10^{12} Ω-cm/pixel. Following the procedure of Ogihara et al. [20] for the evaluation of the plasma time, $t_{\rm p}$, and recombination time, $t_{\rm r}$, and using the model of recombination proposed by Finch et al. [21], $\Delta E_{\rm r}/E_0 = t_{\rm p}/t_{\rm r}$ we obtain a value of $\Delta E_{\rm r}/E_0 \approx 10^{-3}$ for protons of 35 keV of energy. Apart from the model of recombination used to estimate the value of $\Delta E_{\rm r}$, the final argument to uphold that $\Delta E_{\rm r} \approx 0$ for light ions comes from the experimental measurement of the "nuclear stopping defect" carried out by Funsten et al. [22] for protons and He^+ for $E \leq$60 keV, shown in Figure 13. For these two ions and energies, $\Delta E_{\rm n}$ approaches constant saturation values of $\sim$ 0.8 keV (H^+), and 3.2 keV (He^+) which indicates the absence of recombination defect given that $\Delta E_{\rm r}$ could manifest itself as $\Delta E_{\rm r} \propto E$ which is not observed within the range of cited energies. In other words the plasma density, ρ, for low energy and low-Z ions are such that $\rho < \rho_c$, where ρ_c is the critical density [23], [24] and a bias of -75 V is enough to completely sweep the created electron-holes. As a result of the considerations, for our Si detector interacting with low mass, Z=1, ions with $E \lesssim 35$ keV, the PHD is $\Delta E_{PHD} \doteq \Delta E_\mathrm{w} + \Delta E_\mathrm{n}$ or $E' \doteq E_0 - \Delta E_\mathrm{w} - \Delta E_\mathrm{n}$.

For conversion electrons of ^{109}Cd we estimate that $\Delta E_\mathrm{n} \lesssim 50\,\mathrm{eV}$ for the highest electron energy of 87.9 keV. Funsten et al. [25] have estimated a recombination loss of 5×10^{-4} for electrons up to 40 keV. On the other hand, conversion electrons are practically unaffected by ~100 nm thick dead layer, $\Delta E_\mathrm{w} \lesssim 90\,\mathrm{eV}$, accordingly $\Delta E_{PHD} \doteq 0$ within experimental errors, or $E_0 \doteq E'$ for electrons. The same expression is also valid for X-rays.

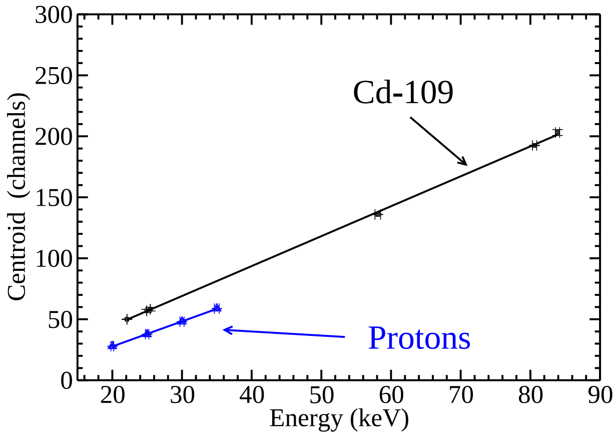

Figure 11: Response of 1 mm thick silicon detector to protons at four energies, and conversion electrons and X-rays from ^{109}Cd.

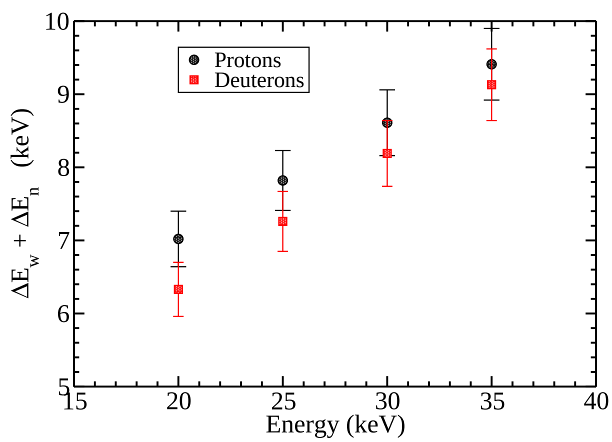

Figure 12: Pulse height defect of protons and deuterons of the large area, 1 mm thick and hexagonal segmented silicon detector, central pixel. The PHD is deduced from Figure 11 for protons.

Figure 11 shows the response of our Si detector to protons, and ^{109}Cd conversion electrons and X-rays. A similar graph is also obtained for deuterons. A linear fit to the proton values from 20 to 35 keV is reasonable, and characterized by a $\chi^2/\mathrm{NDF} = 2.53/4$. The peaks of ^{109}Cd from 20 to 25 keV correspond to X-rays and the electron of 18.5 keV is not observed due to self absorption in the mylar source material which was verified by gamma ray attenuation and also corroborated by Monte Carlo simulation. The pulse height defect $\Delta E_{PHD} = \Delta E_{\rm w} + \Delta E_{\rm n}$, taken from the difference in the measured detector response compared to the ^{109}Cd electron and X-ray response as a function of particle energy, is shown in Figure 12. Results of Figure 12 show that with our 1 mm Si detector and 30 keV protons the energy loss through the dead layer, scattering defect, etc, only amounts to (8.61±0.45) keV leaving 21.4 keV for electron-hole pair production and consecutive collection of charge by the detector.

A possible additional source of defect has been attributed to the average energy, ϵ, required for the creation of an electron-hole pair in silicon. However, Pehl et al. [26] have found that $\epsilon_{\rm e} = \epsilon_\gamma$=(3.67±0.02) eV/pair, where $\epsilon_{\rm e}$ and ϵ_γ are the average electron and photon energy, respectively. On the other hand, Mitchell et al. [27] have measured the ratio of the average energy to create electron-hole pair of deuterons relative to protons in silicon, for energies of ∼1 MeV, obtaining $\epsilon_{\rm d}/\epsilon_{\rm p}$=1.001 ±0.002 which implies that ϵ does not depend strongly on the isotopic mass. Langley [28] has measured the ratio of alphas relative to protons, obtaining the value of $\epsilon_\alpha/\epsilon_{\rm p}$=0.978±0.006, while Bauer and Bortels [29] have measured the ratio of alphas relative to electrons, $\epsilon_\alpha/\epsilon_{\rm e}$=0.985±0.008. Using the last two results we obtain that $\epsilon_{\rm p}/\epsilon_{\rm e}$=1.007± 0.010, that is ϵ_γ, $\epsilon_{\rm e}$, $\epsilon_{\rm p}$, and $\epsilon_{\rm d}$ agree in their main values to the level of $< 1\%$ at room temperature. We expect the same relationship at other temperatures.

5. Computation of the nuclear pulse height defect of protons in silicon by screened coulomb scattering from 1 to 35 keV

A charged particle that is slowed down by Coulomb interactions in silicon loses its energy in two processes, 1) by energy transferred to atomic electrons, $\Delta\eta$, which results in a generation of electron-hole pairs and a subsequent detectable charge, and 2) by energy transferred to the translational motion of the atom $\Delta E_{\rm n}$ which is significant at the end of the particle range. The second process does not produce electron-hole pairs and thus can not be detected through charge collection; the energy transferred to the kinetic energy of the atoms will increase the temperature of the detector. For an incoming particle of energy E, $E = \Delta\eta + \Delta E_{\rm n}$. The calculation of the average transferred energy to recoiling atoms, based on Thomas-Fermi cross sections and dimensionless nomenclature [30, 31], has been carried out by Haines and Whitehead [32]. This energy transferred is also know as nuclear defect and up to the second order of approximation (third order effect is too small) for an amorphous material is given by

$$\langle \Delta E_{\rm n} \rangle = \frac{k_E}{2} \int_0^{\epsilon_0} \left(\epsilon \frac{d\epsilon}{d\rho} \right)^{-1} \times \int_0^{\epsilon^2} Q(t)\, t\, f(t^{\frac{1}{2}})\, \frac{dt}{t^{\frac{3}{2}}}\, d\epsilon \qquad (3)$$

$$Q(\epsilon) = \frac{1}{2\epsilon} \int_0^{\epsilon} \left(\epsilon \frac{d\epsilon}{d\rho} \right)^{-1} \int_0^{\epsilon^2} t\, f(t^{\frac{1}{2}})\, \frac{dt}{t^{\frac{3}{2}}}\, d\epsilon \tag{4}$$

where, ϵ is the dimensionless energy defined by $E = Z_1 Z_2 e^2 (M_1 + M_2)\epsilon / a M_2 \equiv k_E\, \epsilon$; R is the range which is related to the dimensionless range "ρ" by $R = \rho / N \pi a^2 \gamma \equiv k_R\, \rho$; T, the transferred energy related to the dimensionless energy transfer t by $t = \epsilon^2 T / T_m(E)$; $T_m(E)$ is the maximum transferred energy given by $T_m(E) = 4 M_1 M_2 E / (M_1 + M_2)^2 = \gamma E$. The indices 1 and 2 denote the incoming and target particle, respectively, and N is the density of atoms in the substance. The screening radius is $a = 0.8853 a_0 (Z_1^{\frac{2}{3}} + Z_2^{\frac{2}{3}})^{-\frac{1}{2}}$, where $a_0 = 0.529\,\text{Å}$ is the Bohr's radius. $(\frac{d\epsilon}{d\rho})$ is the dimensionless total stopping power. Since both ϵ, and t are dimensionless numbers, $Q(\epsilon)$ is the same as $Q(t)$. The function $f(t^{\frac{1}{2}})$ comes from the Thomas-Fermi cross section which is given by $d\sigma = \pi a^2 f(t^{\frac{1}{2}}) dt / 2 t^{\frac{3}{2}}$ while $f(t^{\frac{1}{2}})$ has the following analytical form [33], $f(t^{\frac{1}{2}}) = \lambda\, t^{\frac{1}{6}} [1 + (2\lambda t^{\frac{2}{3}})^{\frac{2}{3}}]^{-\frac{3}{2}}$, with λ=1.309. The dimensionless stopping power is composed of the nuclear and electronic stopping powers, expressed as

$$\left(\frac{d\epsilon}{d\rho} \right)_{\mathrm{n}} = \frac{1}{2\epsilon} \int_0^{\epsilon^2} t\, f(t^{\frac{1}{2}})\, \frac{dt}{t^{\frac{3}{2}}}\, d\epsilon \tag{5}$$

$$\left(\frac{d\epsilon}{d\rho} \right)_{\mathrm{e}} = k\, \epsilon^{\frac{1}{2}} \tag{6}$$

The proportionality constant, k, in the electronic stopping power has been measured for low energy protons in silicon by Grahmann and Kalbitzer [34] and can also be evaluated using Schiott's equation [35]. The upper range of validity of the nuclear defect is given by $E < Z_1^{4/3} A_1 \times 25\,\text{keV}$ which corresponds to 25 keV for p+Si, 50 keV for d+Si, 250 keV for α + Si, and 23600 keV for Si+Si. Although this upper limit provides the value of 25 keV for protons in silicon, Grahmann and Kalbitzer's work indicates that this limit is extended not only up to 35 keV but even slightly higher in energy. Another significant feature of their result is the linearity in the measured electronic constant with a value of k =1.87±5%.

Results of our nuclear defect computation are shown in Figure 13 and compared with the measured nuclear defect for protons in silicon carried out by Funsten et al. [22]. The agreement is good when Grahmann and Kalbitzer's measured stopping power is used. A dotted line shows the computation of the average nuclear defect using an equivalent electronic constant that resembles Niemann's experimental electronic stopping power from 20 to 35 keV [36]. The range of validity of the electronic stopping power and our interest in the nuclear defect from 15 to 35 keV have limited our computation from 1 to 35 keV. We carried out also a similar computation for low energy deuterons in silicon.

6. Evaluation of dead layer of silicon detectors

Compilation of measured values (including the generated data PSTAR) of the electronic stopping power for low energy protons in silicon is shown in Figure 14 [34, 38, 39, 37, 36, 41].

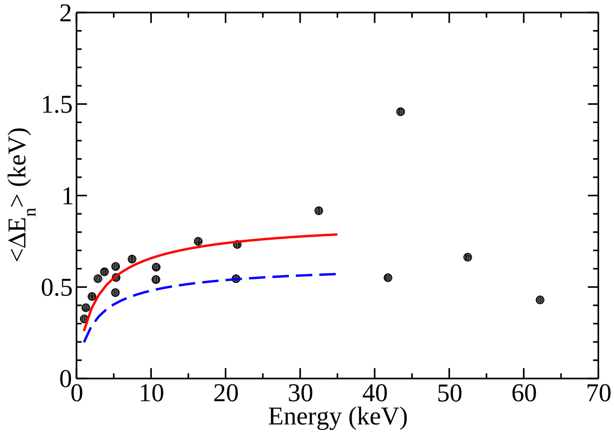

Figure 13: Nuclear defect of low energy protons in Silicon. The computation uses Grahmann and Kalbitzer's measured electronic constant of k=1.87 [34] (solid line). The measured values are taken from the work of Funsten et al. [22] (solid circles). Dashed line is computed with an equivalent electronic stopping power that resembles Niemann's measured stopping power from 20 to 35 keV [36].

For this apparent simple system, a variation of ∼35% is obtained at 30 keV. The dispersion is even higher for theoretical predictions other than the one based in the work of Lindhard, Sharff and Schiott [30, 31]. One of the main difficulties of the theoretical models for the stopping cross section is related to the charge state of the particle inside the material which is certainly difficult to measure [42]. From the experimental point of view, problems inherent with the fabrication of thin foils, thickness determination [40], impurities, foil roughness [39], systematic errors, etc., contribute to the dispersion in the measurement of the electronic stopping cross section. At this point, we are not in a position either to reject or to ignore any experimental electronic stopping power. The argument that supports this criterion is shown in Figure 13 that compares two computed values, based in different stopping powers, with the measured nuc

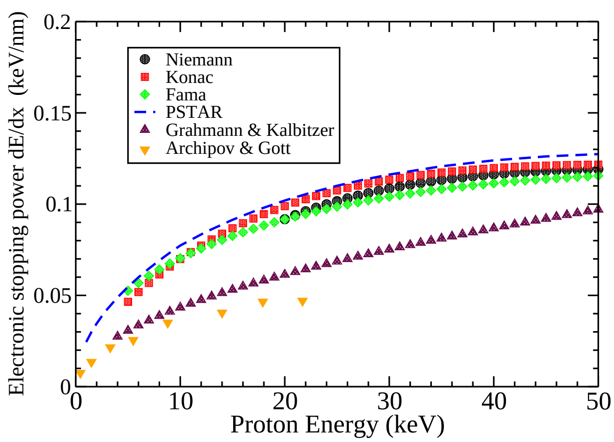

Figure 14: Measured electronic stopping powers for low energy protons in silicon. PSTAR is a generated stopping power based in ICRU report [41].

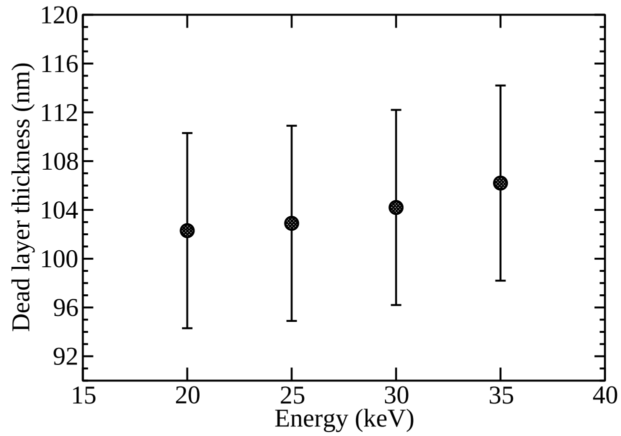

Figure 15: Upper limit of the dead layer thickness for 1 mm thick silicon detector evaluated with Grahmann and Kalbitzer's measured electronic stopping power for protons in silicon [34]. The result in the dead layer is the limiting outcome out of several stopping powers shown in Figure 14.

Figure 15 shows the dead layer of our 1 mm thick silicon detector evaluated with Grahmann and Kalbitzer's electronic stopping power, obtaining a weighted average of (104 ± 4) nm. In the same way, we obtain $\sim$70 nm with the other stopping powers. Using deuteron data, we obtain a dead layer of (75 ± 4) nm with Konac's measured stopping power, and applying the observed absence of isotopic effect in the electronic stopping cross section between protons and deuterons at the same velocity, we obtain (78 ± 5) nm with Fama's data, and (113 ± 5) nm with Grahmann and Kalbitzer; that is, a systematic increase of $\sim$6 nm over the corresponding proton dead layer but with an overall agreement. Due to the sensitivity of low energy ions to probe the dead layer, and given the dispersion in the measured electronic stopping power and measured nuclear defect, we can only indicate that the dead layer is in the range from 70 nm to 110 nm for our 1 mm thick silicon detector.

The measured dead layer of the 0.5 mm thick detector is between 50 nm and 75 nm as examined by protons. The difference in dead layer between 0.5 mm and 1 mm thick detectors might be related to the fabrication process under our requirement for a dead layer of $\lesssim$100 nm.

7. Conclusions

We have characterized large area (108 cm^2), thick (0.5 mm and 1 mm), 127-hexagonal segmented silicon detectors for the neutron beta decay experiments Nab and UCNB, with the initial goal to detect 30 keV protons. The detector properties and development have been done using alphas from ^{241}Am and ^{148}Gd, and 62.5 keV conversion electrons and $\sim$22 keV X-rays from ^{109}Cd. We used the TUNL low energy proton accelerator for proton and deuteron studies. For the 1 mm thick detector we have obtained a bulk leakage current of <0.31 nA/pixel at -6°C, and detected 30 keV protons with the energy resolution of

3.2 keV (FWHM), and signal-to-noise ratio of S/N=(30-8.61)/6.1=3.5. The 1 mm detector dead layer is estimated to be $\lesssim$110 nm thick. The deposited energy was measured by operating the detector at −6°C, with electronics where the FET based preamplifier was directly mounted to the detector pin, followed by a shaping amplifier, and MCA that was operated in peak sensing mode.

In the present work, we achieved the following: 1) detected protons down to 22 keV with the 0.5 mm thick detector which is the noisiest detector compared with the thicker detectors; the low energy limit was set by noise, 2) detected protons and deuterons down to 15 keV with 1 mm thick detector, obtaining the average energy resolution of 3.2 keV for protons, and 3) accomplished a limit of 15 keV proton detection well below 30 keV requirement.

Based on the characterization described in this paper the Nab and UCNB experiments will be further benefited from: 1) operating the detector at lower temperature such as 150 K, operation that minimizes the leakage current, improves the energy resolution, reduces noise, and improves the signal-to-noise ratio, 2) using 2 mm thick large area silicon detectors that are the less noisy detectors, 3) using flash ADCs (FADC) to process the low energy signals, sampling the whole waveform rather than a single peak.

Acknowledgments

This work was supported through Los Alamos National Laboratory LDRD funds. We gratefully acknowledge funding support from NSF through grants PHY-0855610, 0970013, 1205833 and DOE grant DE-FG02-97ER41042. We also acknowledge support from the Office of Nuclear Physics in the Office of Science of the Department of Energy. The first author (ASB) acknowledges the support of P-25, LANL, group leader for extending his research contract.

References

[1] J. Beringer et al. (Particle Data Group), Phys. Rev. D **86** (2012) 010001.

[2] J. Nico, *Neutron beta decay*, J. Phys. G: Nucl. Part. Phys. **36**(2009) 104001.

[3] D. Počanić, et al.,*Nab: Measurement principles, apparatus and uncertainties*, Nucl. Instr. Methods A **611** (2009) 211.

[4] S. Baeßler et al., arXiv:1209.4663 (2012).

[5] W.S. Wilburn et al., *Measurement of the neutrino-spin correlation parameter B in neutron decay using ultracold neutrons*, Revista Mexicana de Física Supplemento **55**, 119 (2009).

[6] R. Alarcon et al., Experiment proposal submitted in November 2007, available at http://nab.phys.virginia.edu/ABBA_proposal_2007.pdf.

[7] PANDA Experiment, Precision Measurement of the Proton Asymmetry in Neutron Decay, proposal, September 22, 2008.

[8] www.micronsemiconductor.co.uk

[9] J.Byrne et al., *Measurement of the Neutron Lifetime by Counting Trapped Protons*, Phys. Lett. **65**, 3, 1990.

[10] J.S. Nico et al., *Measurement of the neutron lifetime by counting trapped protons in a cold neutron beam*, Phys. Rev. C **71**, 055502 (2005).

[11] M. Simson et al., *Detection of low-energy protons using a silicon drift detector*, Nucl. Instr. Methods A **58**, (2007)772-775.

[12] M. Simson et al., *Measuring the proton spectrum in neutron decay—Latest results with aSPECT*, Phys. Lett.,**65**, 3, 1990.
[13] R.L. Cooper et al., *Radiative β decay of the free neutron*, Phys. Rev. C **81**, 035503 (2010).
[14] T.E. Chupp et al., *Search for a T-odd, P-even triple correlation in neutron decay*, Phys. Rev. C **86**, 035505 (2012).
[15] H.P. Mumm et al., *New Limit on Time-Reversal Violation in Beta Decay*, Phys. Rev. Lett. **107**, 102304 (2011).
[16] S.A. Hoedl, A.R. Young, *An electron transparent proton detector for neutron decay studies*, J. Appl. Phys. **99**, 084904(2006).
[17] R.W. Pattie et al., *First Measurement of the Neutron β Asymmetry with Ultracold Neutrons*, Phys. Rev. Lett., **102**, 2009, 012301.
[18] Penelope, A Code System for Monte Carlo Simulation of Electron and Photon Transport. F. Salvat, J. M. Fernandez-Varea, E. Acosta, J. Sempau. Nuclear Energy Agency, 2001.
[19] J. Blachot, Nuclear Data Sheets **107**,355 (2006)
[20] M. Ogihara, Y. Nagashima, W. Galster, T. Mikumo, *Systematic measurements of pulse height defects for heavy ions in surface barrier detectors*, Nucl. Instr. Methods A **251**,313-320(1986).
[21] E.C. Finch, M. Asghar, M. Forte, *Plasma and recombination effects in the fission fragment pulse height defect in a surface barrier detector*, Nucl. Instr. Methods **163**, 467-477(1979).
[22] H.O. Funsten, S.M. Ritzau, R.W. Harper, *Fundamental limits to detection of low-energy ions using silicon solid-state detectors*, Appl. Phys. Lett., Volume 84, Number 18, 2004.
[23] B.D. Wilkins, M.J. Fluss, S.B. Kaufman, C.E. Gross, E.P. Steinberg, *Pulse-height defects for heavy ions in a silicon surface-barrier detector*, Nucl. Instr. Methods **92**, 381-391(1971).
[24] A. Menchaca-Rocha, J.I. Cabrera, R. Alfaro, E. Belmont-Moreno, A. Martinez-Davalos, *A new approach to deal with non-linearities in Si detector response*, Nucl. Instr. Methods B **207**, 356-367(2003).
[25] H.O. Funsten, D.M. Suszcynsky, S.M. Ritzau, R. Korde, *Response of 100% Internal Quantum Efficiency Silicon Photodiodes to 200 eV- 40 keV Electrons*, IEEE Trans. Nucl. Sci., Vol. 44, No. 6, 1997.
[26] R.H. Pehl, F.S. Goulding, D.A. Landis, M. Lenzliger, *Accurate determination of the ionization energy in semiconductor detectors*, Nucl. Instr. Methods **59**, 45-55(1968).
[27] J.B. Mitchell, S. Agami, J.A. Davies, *The use of Si surface barrier detectors for energy calibration of MeV ion accelerators*, Radiat. Eff. **28**, 133-139(1976).
[28] R. A. Langley, *Study of the response of silicon-barrier detectors to protons and alpha particles*, Nucl. Instr. Methods **113**, 109-112(1973).
[29] P. Bauer, G. Bortels, *Response of Si detectors to electrons, deuterons and alpha particles*, Nucl. Instr. Methods A **299** , 205-209(1990).
[30] J. Lindhard, V. Nielsen, M. Scharff, P. V. Thomsen, Kgl. Danske Videnskab Selskab Mat-fys Medd. 33, No 10(1963).
[31] J. Lindhard, M. Scharff, H. E. Schiott, *Range concepts and heavy ion ranges*, Kgl. Danske Videnskab Selskab Mat-fys Medd., 33, No 14, (1963).
[32] E. L. Haines and A. B. Whitehead, *Pulse Height Defect and Energy Dispersion in Semiconductor Detectors*, Rev. Sci. Instrum., Volume 37, Number 2(1966).
[33] D.G. Ashworth and M. Loulavi-kakhki, *Analytical integration of the Thomas-Fermi scattering cross section*, J. Appl. Phys. 55(2), 1984.
[34] H. Grahmann, and S. Kalbitzer, *Nuclear and electronic stopping powers of low energy ions with $Z \leq 10$ in silicon*, Nucl. Instr. Methods **132**, 119-123(1976).
[35] H.E. Schiott, *Approximations and interpolation rules for ranges and range stragglings*, Radiat. Eff., Volume 6, 107-113(1970).
[36] D. Niemann, G. Konac, S. Kalbitzer, *Stopping power measurements of ^{1}H, ^{4}He and ^{14}N in Si in the energy range of 0.02-1 MeV/amu*, Nucl. Instr. Methods B **118**, 11-18(1996).
[37] G.Konac, S. Calbitzer, Ch. Klatt, D. Niemann, R. Stoll, *Energy loss and straggling of H and He ions of keV energies in Si and C*, Nucl. Instr. Methods B 136-138, 159-165(1998).
[38] E.P. Archipov, Yu. V. Gott, *Slowing down of 0.5 to 30 keV protons in some materials*, Soviet Physics

Jetp, Volume 29, Number 4(1969).
[39] M. Fama, G.H. Lantschner, J.C. Eckardt, N.R. Arista, J.E. Gayone, E. Sanchez, F. Lovey, *Energy loss and angular dispersion of 2-200 keV protons in amorphous silicon*, Nucl. Instr. Methods B **193**, 91-96(2002).
[40] P. Bauer, *Stopping power of light ions near the maximum*, Nucl. Instr. Methods B **45**, 673-683(1990).
[41] PSTAR, Stopping-power and range tables for protons, NIST, www.nist.gov
[42] N.R. Arista, *Charge States and Energy Loss of Ions in Solids*, Ion Beam Science, Solved and Unsolved Problems, Part II (2006).